Rolling stones: The motion of a sphere down an inclined plane coated with a thin liquid film

Citation: Bico, J. et al. "Rolling stones: The motion of a sphere down an inclined plane coated with a thin liquid film." Physics of Fluids 21.8 (2009): 082103-8. © 2009 American Institute of Physics

As Published: http://dx.doi.org/10.1063/1.3207884

Publisher: American Institute of Physics

Persistent URL: http://hdl.handle.net/1721.1/61323

Version: Final published version: final published article, as it appeared in a journal, conference proceedings, or other formally published context

Rolling stones: The motion of a sphere down an inclined plane coated with a thin liquid film

J. Bico,[1,2,a)] J. Ashmore-Chakrabarty,[3] G. H. McKinley,[1] and H. A. Stone[3]
[1]*Department of Mechanical Engineering, Hatsopoulos Microfluids Laboratory, Massachusetts Institute of Technology, Cambridge, Massachusetts 02139, USA*
[2]*Physique et Mécanique des Milieux Hétérogènes, ESPCI-ParisTech, Paris 6, Paris 7, UMR CNRS 7635, Paris 75005, France*
[3]*School of Engineering and Applied Sciences, Harvard University, Cambridge, Massachusetts 02138, USA*

(Received 4 March 2009; accepted 13 July 2009; published online 26 August 2009)

A spherical bead deposited on a smooth tilted dry plane wall rolls down the slope under the uniform acceleration of gravity. We describe an analogous experiment conducted using a plane wall that is coated with a thin layer (of order 50–100 μm) of a viscous liquid. The steady motion of the sphere under gravity involves a combination of rotation and sliding. We examine the dependence of the experimentally observed steady translational and rotational speeds on the physical parameters in the system. In particular, the interplay between viscous forces and interfacial forces leads to nontrivial exponents for the scaling of the speeds with the characteristics of the sphere and the viscous liquid. The overhang situation, in which the sphere rolls down the underside of an inclined lubricated plane, is also examined. In this case, the steady motion is still observed for a certain range of angles and bead sizes; that is, the sphere does not always detach from the surface. The adhesive force arises dynamically from the motion of the sphere and can exceed classical quasistatic capillary forces. Such a force should also play a role in other problems of lubrication mechanics such as humid granular flows. © *2009 American Institute of Physics*. [DOI: 10.1063/1.3207884]

I. INTRODUCTION

In his pioneering work on projectile motion Galilei[1] discovered around 1602 that a solid sphere deposited on an inclined plane rolls down with a constant acceleration. Conversely, when the whole experiment is immersed in a viscous fluid, viscous dissipation leads to the steady motion of the sphere.[2,3] We study here an intermediate case where the plane is lubricated with a thin layer of viscous liquid, which introduces capillarity, or interfacial forces, into the problem. While the case of a fully immersed sphere has been described widely as a benchmark for many practical applications ranging from lubrication[4,5] to the flow of suspensions[6] or vesicles,[7] our interfacial situation has received less attention. This configuration may, however, capture some elementary mechanisms relevant to the flow of wet granular media,[8] the rupture of capillary bridges,[9,10] or the classical printer's problem.[11–13] We address several questions: Does the sphere obtain a steady motion? Does it rotate or slide? How does the velocity evolve as a function of the experimental parameters? In particular, will the sphere remain attached to the wall if the tilt angle exceeds 90°?

One common feature of our experiment with the fully immersed situation is with regard to the paradoxical implication of the Stokes equation. At low Reynolds numbers, the flow field is reversible, leading to a symmetrical pressure field around the sphere. This symmetry prevents a normal force from arising and a sphere denser than the surrounding fluid is expected to sink progressively and eventually touch the plane. Although solid-solid friction may be observed experimentally (sliding motion of the sphere), the classical calculation by Goldman *et al.*[14] of the stress and torque experienced by an immersed sphere translating and rotating with a finite gap separation in the vicinity of a plane remains the starting point before taking additional friction effects into account. Some authors have proposed to include roughness effects,[2,15,16] elastic deformation of the solids,[17] pressure-dependence of the fluid properties,[18] or fluid inertia for higher Reynolds numbers.[19,20] In addition, a large pressure drop toward the back of the moving sphere may also initiate the formation of cavitation bubbles, whose presence breaks the symmetry of the Stokes flow and induces a lift force (normal to the plane) on the sphere.[5,11,16,21]

In the following sections, we will first describe our experimental setup in Sec. II and extract the relevant physical parameters through dimensional analysis in Sec. III. After exploring the translation of the sphere as a function of the experimental parameters in Sec. IV, we present some approximate theoretical ideas in Sec. V, and finally we focus on experiments performed in the overhang situation.

II. EXPERIMENTAL SETUP

The experiment is sketched in Fig. 1: A solid sphere is placed on the top of a tilted glass plate 40 cm long that has already been coated with a thin layer of viscous oil. For a given inclination angle α, the position and the rotation of the sphere are recorded with a video camera. The steady translation speed V and the rotation speed Ω are then measured.

The viscous fluids used for most of the experiments are silicone oils with surface tension $\sigma=20.6$ mN/m, density $\rho_f=950$ kg/m^3, and viscosity μ in the range of 1–100 Pa s.

a)Electronic mail: jbico@pmmh.espci.fr.

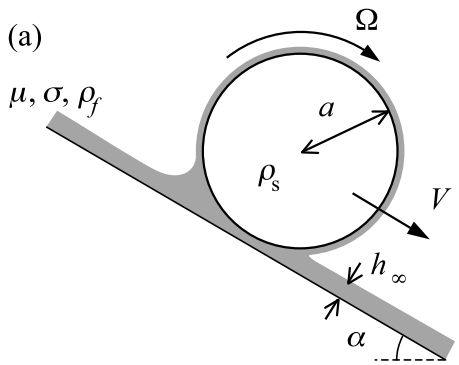

FIG. 1. (Color online) (a) Tilted plate configuration: A sphere is placed on a inclined plate coated with a thin layer of viscous liquid. The motion of the sphere is studied for an imposed tilt angle. (b) Typical experiment illustrating the complex shape of the liquid meniscus around the sphere.

One set of experiments was performed with castor oil, with $\sigma=35$ mN/m, $\rho_f=960$ kg/m^3, and $\mu=0.75$ Pa s. The viscosity of the liquids was determined as a function of temperature with a rheometer (AR1000, TA Instruments) to account for variations in the temperature of the room. The fluid properties are summarized in Table I. The viscous coating is achieved by spreading the viscous liquid with a blade set at a fixed gap from the plate in the range of 50–500 μm. Great care was taken during the spreading to avoid the classical formation of interfacial ribs.[11] Prior to the experiments, the film thickness h_∞ is carefully measured with a displacement confocal micrometer (LT 9000, Keyence). As the plane was tilted, the liquid tended to drain with a typical speed $\rho_f g \sin \alpha h_\infty^2/\mu$. The relative error in the thickness due to drainage can then be estimated by $\rho_f g \sin \alpha h_\infty^2/\mu V$. This error was below 10% for all our experiments. High precision ball bearings with radii a spanning from 1.6 to 16 mm were purchased from hardware suppliers. They were available in different materials with respective solid densities $\rho_s=1.44$ (Delrin®), 2.33 (aluminum), 3.81 (ceramic), 8.34 (chrome steel), 8.52 (brass), and 14.9 (tungsten carbide) g/cm^3. Optical microscopy observations showed that most metal and ceramic spheres had micrometer scale roughness. However, the aluminum and Delrin spheres were found to be significantly rougher. Nevertheless, the maximum amplitude of roughness was determined to be lower than 10 μm for these latter materials. The physical characteristics of the spheres are summarized in Table II.

TABLE I. Fluid material properties.

Liquid	Surface tension (mN/m)	Density (g/cm^3)	Range in viscosity (mPa s)
Silicone oils	20.6	950	1–100
Castor oil	35	960	0.75

TABLE II. Material properties of the spheres.

Material	Density (g/cm^3)	Range in radius (mm)
Tungsten carbide	14.9	2.38–6.35
Brass	8.52	3.18–6.35
Chrome steel	8.34	1.59–15.87
Ceramic	3.81	3.18–15.87
Aluminum	2.33	12.7
Delrin®	1.44	3.18–12.7

The typical experimental positional data reported in Fig. 2 exhibit steady translational and rotational velocities. The sphere is observed to simultaneously rotate (rate Ω) and slide (speed V) during its motion ($a\Omega/V<1$), which suggests the absence of solid-solid friction between the sphere and the wall. This steady motion of the sphere is reached after a short transient regime. A simple estimate of the characteristic distance L_{trans} traveled during this regime is given by $L_{\text{trans}} \sim V^2/g \sin \alpha$, which is found to be less than the sphere perimeter.

A complementary setup was also constructed to confirm the steadiness of the motion: The sphere is placed on the inner face of a rotating drum coated with the viscous liquid. In this case, the height reached by the bead and the corresponding tilt angle α are determined as a function of the velocity V of the base (Fig. 3). Although this apparatus was not suitable for accurate experiments (the sphere rolls on its own track and therefore h_∞ is not carefully controlled), it did prove the steadiness of the phenomenon: After a transient regime the spheres remained in a steady position for several hours. Stable overhang positions were also found. In contrast to the immersed case,[21] the sphere does not detach from the surface over a certain range of the experimental parameters.

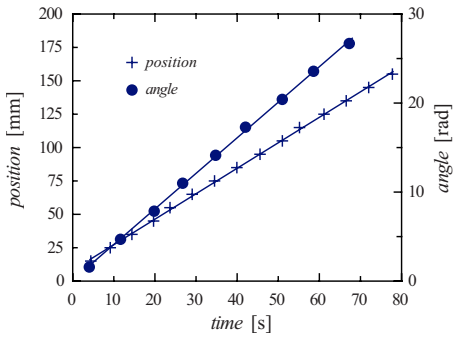

FIG. 2. (Color online) Typical experiment with $\rho_s=14.9$ g/cm^3, $a=3.18$ mm, $h_\infty=150$ μm, $\mu=30$ Pa s, $\sigma=20.6$ mN/m, and $\alpha=13°$ (error bars: 1/30th s for time, 0.2 mm for the position, 0.1 rad for the angle). Steady linear and rotational velocities are measured, $V=1.9$ mm/s, $\Omega=0.34$ rad/s, which leads a sliding coefficient $a\Omega/V=0.57$.

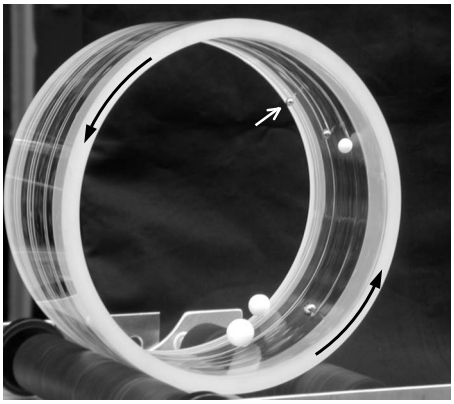

FIG. 3. Drum configuration: The sphere is placed on the inner face of a rotating drum (inner diameter 18 cm) coated with a layer of viscous liquid. Spheres of different radii and densities occupy different angular positions. The position reached by the sphere and the corresponding tilt angle are measured for an imposed drum velocity. The white arrow indicates a sphere rolling steadily in an overhang position.

III. DIMENSIONAL ANALYSIS

The parameters that dictate the independent linear and rotational velocities V and Ω are the angle of inclination α, the sphere radius a and density ρ_s, the film thickness h_∞, the fluid viscosity μ, surface tension σ and density ρ_f, and the gravitational constant g. By dimensional analysis, the whole problem is described by six independent dimensionless parameters. We selected the following combination of these parameters:

$$\frac{\mu V}{\sigma}, \quad \alpha, \quad \frac{\rho_s g a^2}{\sigma}, \quad \frac{h_\infty}{a}, \quad \frac{\rho_f V h_\infty}{\mu}, \quad \frac{\rho_f g h_\infty^2}{\mu V}. \tag{1}$$

The nondimensional velocity, or *capillary number*, $\mathrm{Ca}=\mu V/\sigma$ compares viscous stresses in a meniscus to interfacial stresses. The ratio $\mathrm{Bo}=\rho_s g a^2/\sigma$, referred to as the *Bond number*, compares gravitational forces on the sphere to capillary forces. The quantity $\rho_f V h_\infty/\mu$ is the *Reynolds number* and compares inertia to viscous effects based on the relevant length scale of the liquid flow (h_∞). Finally, the ratio $\rho_f g h_\infty^2/\mu V$ compares the characteristic draining velocity of the fluid to the speed of the sphere. All of our experiments were conducted with a liquid viscous enough, or a film thin enough, to provide low values of the Reynolds number (the maximum value reached in our experiments is 10^{-2}) and slow draining dynamics ($\rho_f g h_\infty^2/\mu V<0.1$, however most common values are orders of magnitude lower). Therefore we assume that the last two parameters in Eq. (1) are not important for determining the motion of the sphere. The assumption of creeping flow is also experimentally confirmed: Translational and rotational velocities are inversely proportional to the fluid viscosity over two decades of viscosity (Fig. 4). We thus expect the sphere motion to depend on three nondimensional parameters,

$$\left(\frac{\mu V}{\sigma}, \frac{a\Omega}{V}\right) = F\left(\alpha, \frac{\rho_s g a^2}{\sigma}, \frac{h_\infty}{a}\right). \tag{2}$$

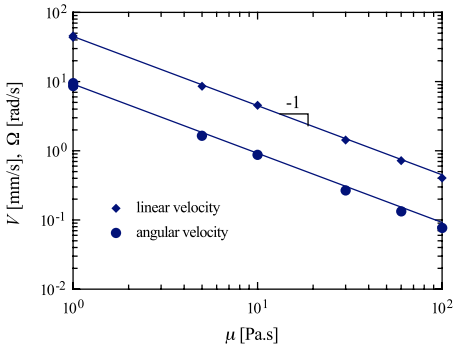

FIG. 4. (Color online) Translational and rotational velocities obtained by the sphere as a function of the liquid viscosity, with $\rho_s=3.8$ g/cm^3, $a=3.18$ mm, $\alpha=24°$, $h_\infty=60$ μm, and $\sigma=20.6$ mN/m (error bars: 5% for μ, 1% for V and Ω).

IV. EXPERIMENTAL RESULTS

A. Different regimes

As expected, the sphere velocity increases for steeper slopes [Fig. 5(a)]. However, three different regimes, related to the detailed shape of the liquid film, are observed successively as the angle is increased. For lower slopes, the meniscus around the sphere is nearly circular. This circular shape is suddenly destabilized, a cusp appears at the rear of the meniscus, and the sphere velocity jumps to a higher value when α reaches a certain threshold [Fig. 5(b)]. Although the threshold angle depends on the sphere size, the transition always occurs for $\mathrm{Ca}\approx 1$, which indicates a strong interplay between viscous and capillary stresses in the meniscus re-

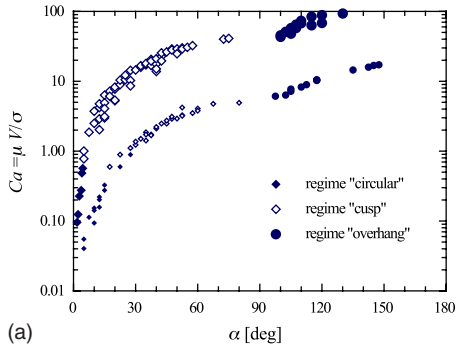

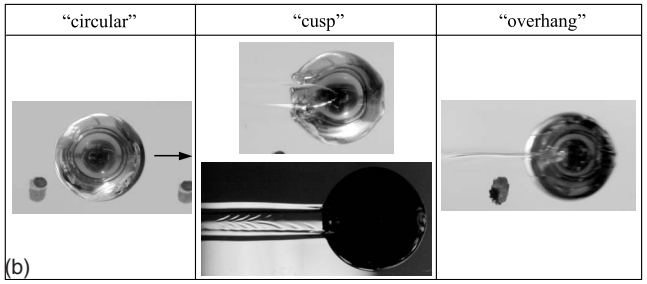

FIG. 5. (Color online) (a) Three distinct kinematic regimes are observed as the slope is progressively increased, $\rho_s=14.9$ g/cm^3, $a=1.59$ mm (small symbols), $a=3.18$ mm (large symbols), $h_\infty=120$ μm, $\eta=30$ Pa s, and $\sigma=20.6$ mN/m (error bars: 2% for α, 5% for Ca). (b) Views from underneath the glass plane illustrating the three regimes: circular meniscus for $\mathrm{Ca}<1$, cusp shape with a tyre print for $\mathrm{Ca}>1$, and overhang case with a single ridge for $\alpha>90°$.

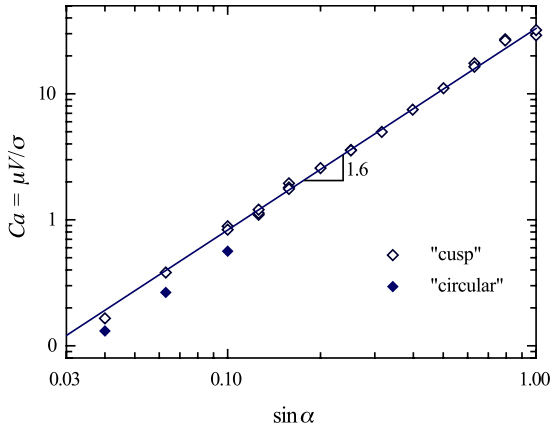

FIG. 6. (Color online) Dependence of the steady translational speed on the angle: V scales with $(\sin\alpha)^{1.6\pm0.05}$ (full line). For $\mu V/\sigma\sim1$ both circular (full symbols) and cusp (open symbols) regimes coexist. Tungsten carbide spheres $a=3.18$ mm, $\rho_s=14.9$ g/cm^3, $h_\infty=120$ μm, and $\sigma=20.6$ mN/m (error bars: 2% for sin α, 5% for Ca).

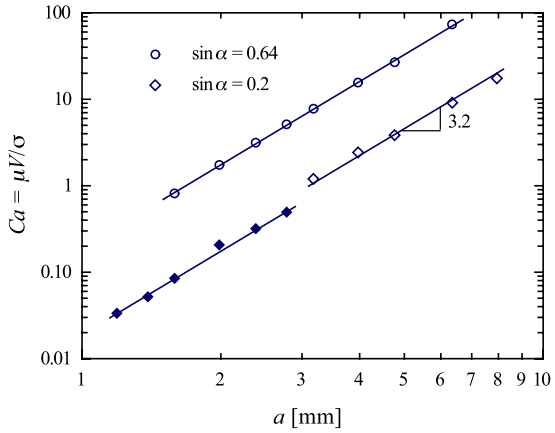

FIG. 7. (Color online) Dependence of the steady translational speed on the sphere radius: V scales with $a^{3.2\pm0.05}$ (full lines). $\rho_s=7.8$ g/cm^3, $h_\infty=90$ μm, $\sigma=20.6$ mN/m, upper data $\alpha=40°$, and lower data $\alpha=11.5°$ (error bars: $<1\%$ for a, 5% for Ca). In the later case, a transition from circular (full symbols) to cusp (open symbols) regimes is observed for $\mathrm{Ca}\simeq1$, which leads to a jump (of 60%) in velocity.

gion when the cusp appears. Oblique ridges are also observed between two parallel wedges in the wake of the sphere, leading to the appearance of a "tyre print." This interfacial instability is reminiscent of the printer's ribbing instability that has been described extensively in literature.[11,12] In the printer's situation, a viscous liquid is carried through the gap h between two counter-rotating rollers of radius R: For low rotation speeds, the liquid splits into two uniform coating sheets, but for high speeds the sheets are regularly ridged. Following Ref. 12 the onset of instability is then experimentally found when $\mathrm{Ca}\sim62h/R$ (Fig. 7 in the reference), which is in qualitative agreement with a linear stability analysis of the liquid flow. Although the flow geometry is different in the case of a sphere rolling on a plane, taking $h\sim h_\infty$ would lead to the criterion $\mathrm{Ca}\approx O(1)$ for the printer's instability to develop, which confirms the similarity of the two instabilities. Close to the transition, states with circular or cusp shapes coexist in a narrow window of capillary number (or tilt angle). Within this window, the observed state depends on the initial conditions.

Finally, a third, overhang regime is observed when the inclination angle is above 90° (the maximum bound depends on the radius of the sphere as will be discussed in Sec. V B). The shape of the liquid-air interface undergoes another instability: The cusp vanishes and a single wedge replaces the tyre print previously observed [Fig. 5(b)].

B. Dependence on the physical parameters

Before further theoretical considerations, we examine here the evolution of the sphere velocity with the relevant physical parameters (specifically α, a, ρ_s, h_∞, and σ). The results are presented in Figs. 6–8 in terms of a dimensionless speed or capillary number. In classical sedimentation dynamics, the balance of the gravitational force ($\approx a^3\rho_s g\sin\alpha$) with viscous drag ($\approx a\mu V$) leads to a terminal speed proportional to $a^2\rho_s g\sin\alpha/\mu$. However our measurements show stronger power-law dependencies over two decades in sin α and one order of magnitude in a and ρ_s: The velocity V scales with $(\sin\alpha)^{1.6\pm0.05}$ (Fig. 6), with $a^{3.2\pm0.05}$ (Fig. 7), and with $\rho_s^{1.35\pm0.05}$ (Fig. 8). The different exponents for sin α and ρ are also counterintuitive, at least based on naive physical inspection, and indicate the importance of the deformation of the liquid-air interface. The results bring to mind the problem of liquid droplets running down a nonwetted surface. In that situation the translation speed of the droplet is found to be proportional to $\sin\alpha/(\rho g)^{1/2}$.[22,23] Also, we note that although the transition from "circular" to "cusp" regimes for $\mu V/\sigma\sim1$ leads to a jump in velocity, this jump does not affect the scaling exponents.

The combination of these experimental scaling laws with the dimensional analysis from Sec. III suggests a scaling of V with $(h_\infty)^{-0.5}$. According to this prediction, thicker films lead to a slower motion of the sphere, in qualitative agreement with experimental data. However the detailed motion of the sphere was observed to be more complex: While h_∞ remains small in comparison with a ($a/h_\infty>10$), $V\propto(h_\infty)^{-0.5\pm0.05}$ as expected (Fig. 9). Erratic motions (unsteady velocity, irregu-

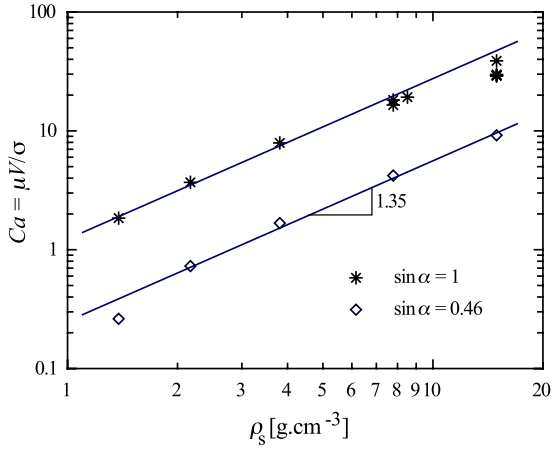

FIG. 8. (Color online) Dependence of the steady translational speed on the sphere density: V scales with $\rho_s^{1.35\pm0.05}$ (full line). Both experiments correspond to cusp regimes (error bars: 1% for ρ_s, 5% for Ca).

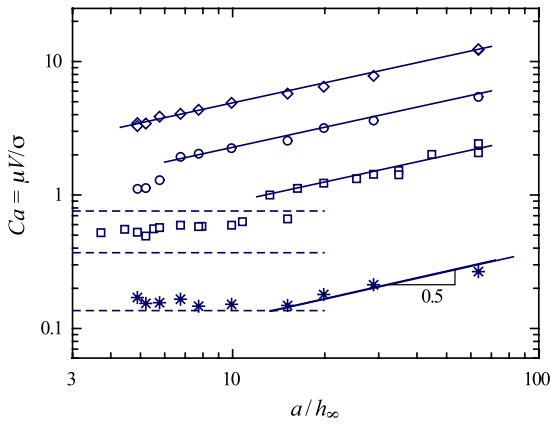

FIG. 9. (Color online) Dependence of the steady translational speed on the film thickness. While $a/h_\infty > 10$, V scales with $h_\infty^{-0.5\pm0.05}$ (full lines). Comparison with the fully immersed case adapted from Ref. 21 (dashed lines) when V eventually becomes independent of h_∞. The four series of experiments were conducted with $\alpha = 23.5°$, $a = 3.18$ mm, ($\diamond$) $\rho_s = 14.9$ g/cm^3, ($\circ$) $\rho_s = 7.8$ g/cm^3, ($\square$) $\rho_s = 3.8$ g/cm^3, and ($*$) $\rho_s = 1.4$ g/cm^3 (error bars: 10% for a/h_∞, 5% for Ca).

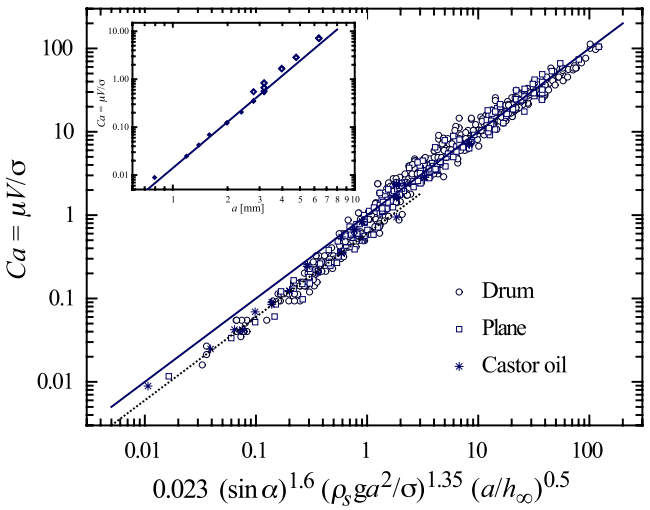

FIG. 10. (Color online) Final collapse of the experimental data for $\alpha \leq 90°$. The ranges for the physical parameters are 1.6 mm $\leq a \leq$ 16 mm, 1.4 g/cm$^3 \leq \rho_s \leq$ 14.9 g/cm^3, 1 Pa s $\leq \eta \leq$ 100 Pa s, and $0.02 \leq \sin\alpha \leq 1$ (error bars: 10% for the abscissa, 5% for Ca). The liquids used for most experiments are silicone oils ($\sigma = 20.6$ mN/m), but a series of data were obtained with castor oil [($*$) $\sigma = 35$ mN/m]. For Ca > 1 (cusp regime), the linear velocity of the sphere scales as $\mu V/\sigma = 0.023(\sin\alpha)^{1.6}(\rho_s g a^2/\sigma)^{1.35}(a/h_\infty)^{0.5}$ (full line). The same scaling is observed for Ca < 1 (circular regime), but the prefactor becomes 0.014 (dashed line). Inset: sphere velocity vs radius with a film of castor oil.

lar spinning) were sometimes observed for thicker films, which suggests intermittent friction of the sphere with the plane. This last regime is expected to match the fully immersed situation when h_∞ eventually reaches the order of a. Following the recent work from Ref. 21, the values of V are expected to depend on the existence of cavitation bubbles, and to be proportional to the sedimentation velocity $a^2(\rho_s - \rho_f)g/\mu$ corrected by a function of α. Our experimental results for thick films ($a/h_\infty < 10$) are in agreement with this limit. Indeed, the steady velocity of the sphere (for nonerratic experiments) becomes independent of the film thickness when $a/h_\infty < 10$, and the translation speed extracted from the work of Ashmore *et al.* (where $\rho_s - \rho_f$ has been replaced by ρ_s since buoyancy is negligible in our experiments) gives the right order of magnitude of the experimental velocity (dashed lines in Fig. 9).

To conclude this section, the different empirical power-law dependencies observed for the nondimensional groups are combined. As shown in Fig. 10, the large collection of experimental data collapses into the general scaling law

$$\eta V/\sigma \sim (\sin\alpha)^{1.6}(\rho_s g a^2/\sigma)^{1.35}(a/h_\infty)^{0.5}, \tag{3}$$

with an accuracy of 0.05 for each exponent, and prefactors 0.014 and 0.023 in the circular and cusp regimes, respectively. Both regimes coexist in the vicinity of Ca $\simeq 1$. Equation (3) predicts a dependence of the speed on the liquid surface tension $V \propto \sigma^{-0.35}$. A last series of experiments was finally conducted with a liquid of different surface tension (castor oil, $\sigma = 35$ mN/m) and was in good agreement with the other results (inset in Fig. 10). The validity of these relations is limited to thin lubricant coatings ($a/h_\infty > 10$). Thicker coatings appear to tend to the immersed situation where the velocity is given by $\mathrm{Ca} \sim f(\alpha)a^2(\rho_s - \rho_l)g/\sigma$. However, the erratic motion of the sphere often observed in this thick-layer regime also suggests that solid friction (i.e., sphere-wall contact) becomes an important ingredient of the motion. Lower bounds for h_∞ are also obviously reached when h_∞ or the gap between the sphere and the wall is comparable to the surface roughness (of micron scale). Although Eq. (3) is limited to $\alpha \leq 90°$, overhang situations are also observed. The speed of the overhang spheres follow a different law that will be described in Sec. V B.

C. Sliding versus rotation

The sliding coefficient, $a\Omega/V$, indicates if the sphere slides ($a\Omega/V = 0$) or rolls ($a\Omega/V = 1$) down the inclined plane. In the fully immersed situation this coefficient tends to the asymptotic value 0.25.[21] In the present configuration, $a\Omega/V$ reaches much higher values ($a\Omega/V \sim 0.6$). As the velocity of the sphere was increased, we observed two successive regimes, with a transition corresponding to Ca ~ 1 (Fig. 11). For lower velocities, the sliding ratio was close to unity and the motion of the sphere was partially erratic, revealing transient solid friction between the sphere and the wall. In this first regime $a\Omega/V$ was found to decrease as Ca increased. Beyond the transition (Ca > 1), the values for the sliding coefficient tended to scatter around an average value. This value was found to slightly increase with the ratio a/h_∞ (Fig. 12). As intuition would suggest, thicker lubricating layers resulted in an increase in sliding. Finally, the effect of the sphere density was explored: Less dense spheres tend to slide more than denser ones (Fig. 12). These observations confirm the important lubricating role played by the viscous fluid.

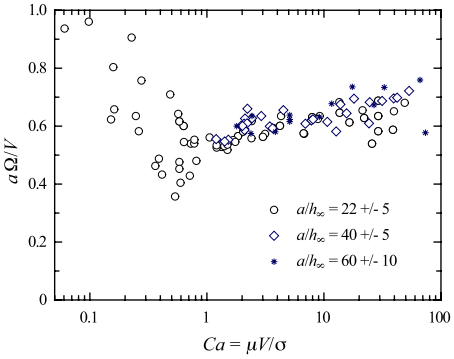

FIG. 11. (Color online) Sliding coefficient $a\Omega/V$ as a function of the dimensionless sphere velocity (error bars: 5% for Ca, 3% for $a\Omega/V$). In the first regime, the value of $a\Omega/V$ is close to unity and the erratic motion of the sphere often observed experimentally indicates transient contact between the sphere and the wall. Note that data corresponding to different experimental parameters have been combined in the same sets of ranges of a/h_∞. We believe the slight dependence of the sliding coefficient on multiple parameters may explain the observed scatter.

V. DISCUSSION

A. Common rolling regime

We have attempted to provide theoretical arguments to rationalize the experimentally measured scaling laws. Unfortunately, the flow is a three-dimensional free-surface problem, which introduces many complexities and even thinking about two-dimensional variants of this finite capillary number problem appears nontrivial. Nevertheless, we believe that some of our thoughts are worth sharing. One approach is to use the steady-state force and torque balances to obtain the three unknown quantities V, Ω, and the gap thickness h_0 between the sphere and the plane (see Fig. 13). For example, the flow in the narrow gap under the sphere can be considered similar to the lubrication calculation of Goldman *et al.*[14] However, the presence of the meniscus brings additional effects into our system. For instance, the cusp observed at the rear of the sphere breaks the symmetry of the Stokes flow and results in a finite normal force. Capillary forces also tend to attract the sphere toward the wall in the same manner as the cohesion of sand castles relies on capillary bridges between sand grains.[24] Interestingly, the corresponding capillary force is almost constant while the volume of the liquid bridge is small. (In practice, the capillary force eventually vanishes when the volume of liquid is not enough to fill the space between the asperities of the surfaces roughness.[24] In this situation the vanishing force only relies on a decreasing number of minute capillary bridges between asperities.) In the case of a smooth nonmoving sphere and a plane the adhesion force is given by[25] $F_{\mathrm{cap}}=4\pi a\sigma$. In the present rolling case, the shape of the meniscus is more complex and the expression for F_{cap} should certainly be corrected. In addition to the normal capillary attraction, the asymmetry of the meniscus may finally lead to distributions of tangential forces and a torque acting on the sphere. In this way, the forms for the tangential force and normal force balances, as well as the torque balance around the center of the sphere should read, respectively,

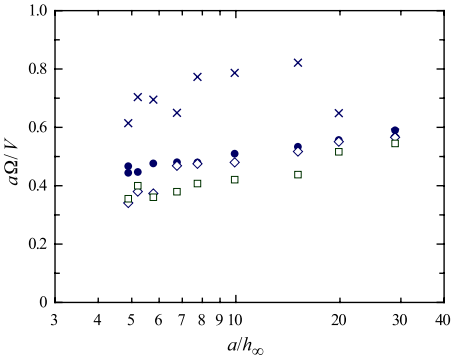

FIG. 12. (Color online) The sliding coefficient $a\Omega/V$ increases when the relative thickness of the liquid is reduced and as the solid density is increased: (●) (ρ_s=14.9 g/cm^3), (◇) (ρ_s=7.8 g/cm^3), (□) (ρ_s=3.8 g/cm^3), and (×) (ρ_s=1.4 g/cm^3). σ=20.6 mN/m and α=23.5° (error bars: 5% for a/h_∞, 3% for $a\Omega/V$). The rotation of the lighter spheres sliding at low values of Ca tended to be erratic and poorly reproducible, which is probably due to intermittent solid friction.

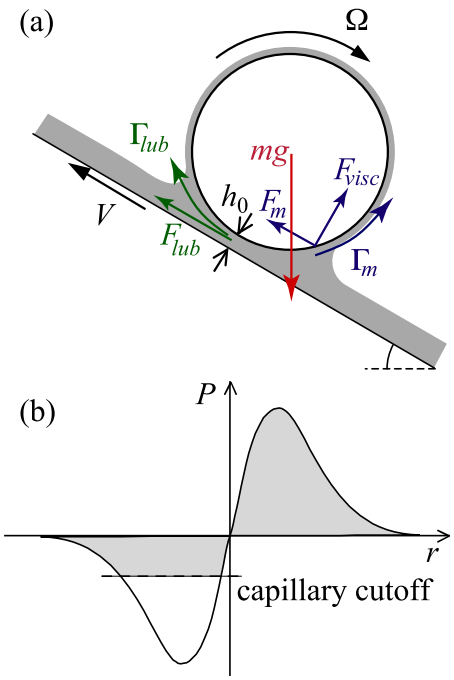

FIG. 13. (Color online) (a) In the reference frame of the sphere, force and torque distributions acting on the sphere. (b) The symmetry of the pressure profile under the sphere is expected to be broken by a capillary cutoff, which would lead to a positive normal force.

$$\frac{4}{3}\pi a^3\rho_s g\,\sin\alpha=\frac{16\pi}{5}\mu(V-a\Omega)a\,\ln(a/h_0)+F_m, \tag{4}$$

where F_m represents the capillary force arising from the asymmetry of the meniscus,

$$\tfrac{4}{3}\pi a^3\rho_s g\,\cos\alpha=F_{\mathrm{cap}}+F_{\mathrm{visc}}, \tag{5}$$

where F_{visc} is the viscous lubrication force resulting from a nonsymmetric Stokes flow, and

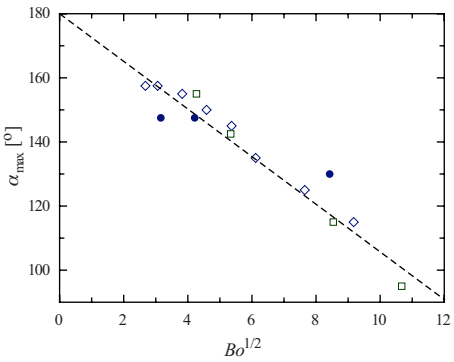

FIG. 14. (Color online) Maximum tilt angle of the slope α_{max} that allows steady translational motion and dynamic capillary adhesion of the sphere vs Bond number, $Bo=\rho_s g a^2/\sigma$. The results suggest a window in the size of the adhering spheres. (●) (ρ_s=14.9 g/cm^3), (◇) (ρ_s=7.8 g/cm^3), and (□) (ρ_s=3.8 g/cm^3) and (h_∞=120 μm). Error bars: 2% for $Bo^{1/2}$, 5° for α_{max}.

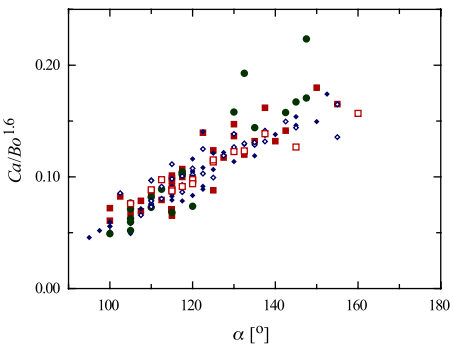

FIG. 15. (Color online) Velocity of the sphere vs inclination angle in the overhang regime, for which we find an empirical scaling $Ca/Bo^{1.6}=f(\alpha)$. (●) (ρ_s=14.9 g/cm^3), (◇) (ρ_s=7.8 g/cm^3), (□) (ρ_s=3.8 g/cm^3), full symbols h_∞=120 μm, and open symbols h_∞=60 μm (error bars: 5° for α, 8% for $Ca/Bo^{1.6}$).

$$0=\frac{4\pi}{5}\mu(V-a\Omega)a^2\ln(a/h_0)+\Gamma_m, \tag{6}$$

where Γ_m is the torque on the sphere due to the asymmetry of the meniscus. Lacking a detailed description of the flow, we are unable to estimate the contribution of the meniscus in this complex geometry.

With the hope of simplifying the geometry, we finally considered experimentally the case of rolling cylinders. However the motion was not steady: Some liquid coating the surface of the cylinder eventually accumulated in the meniscus in front of the cylinder leading to a growing bulge. As the bulge grew, the motion of the cylinder became unsteady: The direction of the cylinder axis oscillated, which led to a zigzagging motion down the plane. In the case of the sphere, the coating fluid can flow azimuthally around the sides and does not accumulate in front of the sphere. The last observation reinforces the importance of the three dimensionality of the flow for our problem.

B. Overhang regime

For a certain range of parameters, spheres where observed to roll at steady speeds down overhanging planes with inclinations greater than 90°. Although interfacial forces would sustain light beads, we observed heavy spheres steadily rolling in an inverted configuration (e.g., bead indicated by an arrow in Fig. 3). Comparing the capillary adhesion force to the weight of the sphere simply yields the Bond number, $Bo=\rho_s g a^2/\sigma$. We focus here on this counterintuitive regime of overhanging heavy spheres, where $Bo\cos\alpha>3$ which do not occur in the fully immersed situation.[21]

The maximum slope angle α_{max} allowing the steady motion of an overhanging sphere was determined as a function of Bo (Fig. 14). As expected α_{max} tends to 90° for heavy spheres and to 180° for lighter ones. Our preliminary experimental data suggest a linear dependence of α_{max} with $Bo^{1/2}$, with a maximum value of order $Bo\approx 150$, which corresponds to $a\simeq 6$ mm for a steel sphere. Counterintuitively, the linear velocity was not a maximum for $\alpha=90°$, but was found to increase with further increases in the slope. An empirical scaling $Ca/Bo^{1.6}=f(\alpha)$ collapses the experimental data to a master curve (Fig. 15).

Although a comprehensive interpretation of these results remains an open question, we believe that the adhesive force results from the interplay of viscous effects and capillarity. In particular, the free rotation of the sphere is found to be necessary for the adhesion of the sphere on the underside of an inclined wall. Experiments were carried out with pairs of spheres of the same radius, a regular sphere of uniform density, and a lighter one where additional ballast had been concentrated on its surface to compensate for the weight difference. The ballast prevents the second sphere from rotating and the sphere eventually detaches for any angle higher than 90°. The mechanism for this dynamic adhesion may rely on a steady detachment in the rear part of the meniscus, leading to a viscous restoring force.[9,10] Our experiments are reminiscent of an interesting study by Barquins[26] in the context of adherence and friction on an elastic body. A rigid cylinder was observed to roll down an elastic incline at a constant velocity. An overhang motion was also observed, but the relationship of the velocity as a function of the tilt angle was symmetric with respect to the vertical (the velocity first increases until α reaches 90°, then decreases). Although there are some common features with our experiment, the dissipative mechanisms are different. In the case of the elastic substrate, the dynamics are mainly controlled by rupture energy at the rear of the cylinder (where most of the energy is dissipated), while the extension of the contact area between the substrate and the cylinder relies on adhesion forces.

VI. CONCLUSION

A sphere deposited on an incline coated with a thin layer of viscous fluid was observed to move down the plane at a constant velocity. During its displacement, the sphere slides as it rolls, which confirms the lubricating role of the thin viscous layer. The steady translational descent velocity was explored as a function of the physical variables of the problem: sphere radius and density, thickness of the liquid layer, viscosity, surface tension, and inclination angle of the plane. An empirical scaling law with nonintuitive exponents pro-

vides a collapse of the experimental data onto a single master curve over four orders of magnitude in velocity. For a limited range of inclinations greater than 90° the sphere can overhang and steadily roll down underneath the coated plane. In this last regime, the adhesion force proves to be mainly dependent on viscous effects. Due to the complexity of the three-dimensional free-surface flow, we were not able to provide a theoretical framework to quantify these experimental results. Additional insights may be gained with the help of numerical simulations or a more detailed theoretical description of the problem. From the experimental point of view, a precise estimation of the small gap separating the sphere from the plane should also provide useful information on the dynamics. We hope that our preliminary work will motivate further studies of similar problems.

ACKNOWLEDGMENTS

This work was supported in part by a Rohsenow Fellowship from the Department of Mechanical Engineering of MIT. We are very grateful to V. Entov (deceased), T. Mullin, and J. Seddon for encouragement and useful suggestions.

[1] G. Galilei, *Dialogues Concerning Two New Sciences* (Macmillan, New York, 1914).
[2] J. R. Smart, S. Beimfohr, and D. T. Leighton, "Measurement of the translational and rotational velocities of a noncolloidal sphere rolling down a smooth inclined plane at low Reynolds-number," Phys. Fluids A **5**, 13 (1993).
[3] Y. J. Liu, J. Nelson, J. Feng, and D. D. Joseph, "Anomalous rolling of spheres down an inclined plane," J. Non-Newtonian Fluid Mech. **50**, 305 (1993).
[4] O. Reynolds, "On the theory of lubrication and its application to Mr. Beauchamp Tower's experiments, including an experimental determination of the viscosity of olive oil," Philos. Trans. R. Soc. London **177**, 157 (1886).
[5] D. Dowson and C. M. Taylor, "Cavitation in bearings," Annu. Rev. Fluid Mech. **11**, 35 (1979).
[6] Y. Zhao, K. P. Galvin, and R. H. Davis, "Motion of a sphere down a rough plane in a viscous fluid," Int. J. Multiphase Flow **28**, 1787 (2002).
[7] M. Abkarian, C. Lartigue, and A. Viallat, "Motion of phospholipidic vesicles along an inclined plane: Sliding and rolling," Phys. Rev. E **63**, 041906 (2001).
[8] S. Nowak, A. Samadani, and A. Kudrolli, "Maximum angle of stability of a wet granular pile," Nat. Phys. **1**, 50 (2005).
[9] M. J. Matthewson, "Adhesion of spheres by thin liquid films," Philos. Mag. A **57**, 207 (1988).
[10] O. Pitois, P. Moucheront, and X. Chateau, "Liquid bridge between two moving spheres: An experimental study of viscosity effects," J. Colloid Interface Sci. **231**, 26 (2000).
[11] J. R. A. Pearson, "The instability of uniform viscous flow under rollers and spreaders," J. Fluid Mech. **7**, 481 (1960).
[12] E. Pitts and J. Greiller, "The flow of thin liquid films between rollers," J. Fluid Mech. **11**, 33 (1961).
[13] M. Rabaud, "Interface dynamics in the printer instability," Ann. Phys. **19**, 659 (1994).
[14] A. J. Goldman, R. G. Cox, and H. Brenner, "Slow viscous motion of a sphere parallel to a plane wall. I. Motion through a quiescent fluid," Chem. Eng. Sci. **22**, 637 (1967).
[15] K. P. Galvin, Y. Zhao, and R. H. Davis, "Time-averaged hydrodynamic roughness of a noncolloidal sphere in low Reynolds number motion down an inclined plane," Phys. Fluids **13**, 3108 (2001).
[16] A. N. Prokunin, "On a paradox in the motion of a rigid particle along a wall in a fluid," Fluid Dyn. **38**, 443 (2003).
[17] R. Gohar, *Elastohydrodynamics*, 2nd ed. (Imperial College Press, London, 2001).
[18] P. L. Kapitza, *Collected Papers of P. L. Kapitza* (Pergamon, Oxford, 1965), Vol. II.
[19] G. P. Krishnan and D. T. Leighton, "Inertial lift on a moving sphere in contact with a plane wall in a shear-flow," Phys. Fluids **7**, 2538 (1995).
[20] M. R. King and D. T. Leighton, "Measurement of the inertial lift on a moving sphere in contact with a plane wall in a shear flow," Phys. Fluids **9**, 1248 (1997).
[21] J. Ashmore, C. del Pino, and T. Mullin, "Cavitation in a lubrication flow between a moving sphere and a boundary," Phys. Rev. Lett. **94**, 124501 (2005).
[22] L. Mahadevan and Y. Pomeau, "Rolling droplets," Phys. Fluids **11**, 2449 (1999).
[23] D. Richard and D. Quéré, "Viscous drops rolling on a tilted non-wettable solid," Europhys. Lett. **48**, 286 (1999).
[24] T. C. Halsey and A. J. Levine, "How sandcastles fall," Phys. Rev. Lett. **80**, 3141 (1998).
[25] J. Israelachvili, *Intermolecular and Surface Forces*, 2nd ed. (Academic, London, 1992).
[26] M. Barquins, "Adherence, friction and contact geometry of a rigid cylinder rolling on the flat and smooth surface of an elastic body," J. Nat. Rubber Res. **5**, 199 (1990).